Eurographics Symposium on Rendering 2018
T. Hachisuka and W. Jakob
(Guest Editors)

Volume 37 (2018), Number 4

A Physically-based Appearance Model for Special Effect Pigments Supplemental Document

Jie Guo, Yanjun Chen, Yanwen Guo and Jingui Pan

State Key Lab for Novel Software Technology, Nanjing University

1. Introduction

This document is supplemental to the paper entitled *A Physically-based Appearance Model for Special Effect Pigments*. In the following sections, we provide derivations of some important formulas, detailed discussions of some parameters, and more comparisons.

2. Influence of the Order Offset of OPD

When a light is incident on a thin film and reflected by both the upper and lower boundaries, an iridescent appearance will occur and changes w.r.t. the optical path different (OPD) between the primary and secondary light paths. As the light may be internally reflected multiple times before it leaves the thin film, there would be different orders of OPD. The first-order OPD is $\mathcal{D} = 2\eta_l d \cos\theta_2$, while the kth order OPD is $k\mathcal{D}$. According to the spectral Airy reflectance in [BB17], the spectral Airy term F is given by

$$F = C_0 + 2\sum_{m=1}^{+\infty} C_m \cos(m(2\pi\nu\mathcal{D} + \phi)) \tag{1}$$

where m denotes the order offset of OPD, ν is the inverse of the wavelength, and ϕ represents the net phase shift caused by light reflection from both the upper and lower boundaries. C_0 (resp. C_m) is computed by summing interferences for all pairs of light paths with an offset of zero (resp. m) in orders. Please refer to [BB17] for detailed descriptions of C_0, C_m and ϕ.

As we mentioned in our paper, we only consider order offset of zero and one, i.e.,

$$F = C_0 + 2C_1 \cos(2\pi\nu\mathcal{D} + \phi) \tag{2}$$

since higher orders make little contribution. This is verified in Fig. 1 where we render a ball under constant environmental lighting with three values of η_l (the refractive index of the thin film). The OPD at normal incidence is set as $\mathcal{D} = 2\eta_l d = 1.6e-6$ while the refractive index of the conductive base is set as $1.1 + 1.5i$. From the visual comparison in each row, we see that the differences between $m = 1$ an $m = 3$ are subtle under different parameter settings.

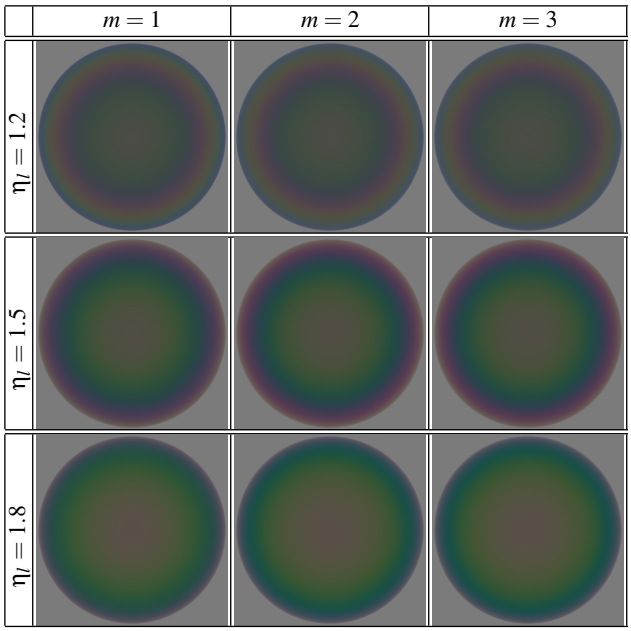

Figure 1: *Influence of the order offset m under different parameter settings.*

3. Derivation of Eq. 11

In our paper, we fit four isotropic Gaussians to the CIE XYZ sensitivity functions. Note that two Gaussians are required for the X channel. The fitting objective is give by

$$S_c(\nu) = A_c e^{-\frac{(\nu - a_c)^2}{2\sigma_c^2}} \tag{3}$$

where A_c, a_c and σ_c are the fitting parameters for each channel. Table 1 lists the fitting results.

Similar to that of [BB17], we perform the spectral integration in the Fourier domain. Specifically, the Fourier transform of Eq. 3 is given by

$$\mathcal{F}(S_c)(f) = A_c\sqrt{2\pi\sigma_c^2}\, e^{-2\pi^2\sigma_c^2 f^2} e^{-2\pi i f a_c} \tag{4}$$

© 2018 The Author(s)
Computer Graphics Forum © 2018 The Eurographics Association and John Wiley & Sons Ltd. Published by John Wiley & Sons Ltd.

	A_c	a_c	σ_c
X_1	3.8789e-13	1.6810e+06	9.3035e+04
X_2	6.8922e-14	2.2399e+06	9.5165e+04
Y	3.1255e-13	1.7953e+06	1.3642e+05
Z	3.7110e-13	2.2084e+06	1.1500e+05

Table 1: *Fitting results for the CIE XYZ sensitivity functions. Note that two Gaussians are required for the X channel.*

parameterized by f. It is then normalized, yielding:

$$\tilde{\mathcal{F}}(S_c)(f) = e^{-2\pi^2\sigma_c^2 f^2} e^{-2\pi i f a_c}. \tag{5}$$

This ensures that $\tilde{\mathcal{F}}(S_c)(0) = 1$. The Fourier transform of the spectral Airy term is give by

$$\mathcal{F}(F)(f) = C_0\delta(f) + C_1[e^{i\phi}\delta(f-\mathcal{D}) + e^{-i\phi}\delta(f+\mathcal{D})]. \tag{6}$$

In the Fourier domain, the spectral integration becomes

$$F_c = \int \mathcal{F}(F)(f)\tilde{\mathcal{F}}(S_c)(f)^\star \mathrm{d}f \tag{7}$$

in which * represents the complex conjugate. Substituting Eq. 5 and Eq. 6 into Eq. 7 and let $\tilde{\mathcal{F}}(S_c)(f)^\star = \tilde{\mathcal{F}}(S_c)(-f)$, we get

$$F_c = C_0 + 2C_1\cos(\phi + 2\pi a_c\mathcal{D})e^{-2\pi^2\sigma_c^2\mathcal{D}^2}. \tag{8}$$

Substituting $\mathcal{D} = 2\eta_l\cos\theta_2 d$ into the above equation results in Eq. 11 in the paper.

3.1. Special Consideration for the X Channel

As we mentioned, we fit two Gaussians to the X Channel, i.e.,

$$S_X(\nu) = A_{X1}e^{-\frac{(\nu-a_{X1})^2}{2\sigma_{X1}^2}} + A_{X2}e^{-\frac{(\nu-a_{X2})^2}{2\sigma_{X2}^2}}. \tag{9}$$

This causes some differences for the Fourier transformation and the normalization. Its Fourier transformation is

$$\begin{aligned}\mathcal{F}(S_X)(f) = &A_{X1}\sqrt{2\pi\sigma_{X1}^2}e^{-2\pi^2\sigma_{X1}^2 f^2}e^{-2\pi i f a_{X1}}\\ &+A_{X2}\sqrt{2\pi\sigma_{X2}^2}e^{-2\pi^2\sigma_{X2}^2 f^2}e^{-2\pi i f a_{X2}}.\end{aligned} \tag{10}$$

To normalize the above equation ensuring $\tilde{\mathcal{F}}(S_c)(0) = 1$, we get

$$\begin{aligned}\tilde{\mathcal{F}}(S_X)(f) = &k_1 e^{-2\pi^2\sigma_{X1}^2 f^2}e^{-2\pi i f a_{X1}}\\ &+k_2 e^{-2\pi^2\sigma_{X2}^2 f^2}e^{-2\pi i f a_{X2}}.\end{aligned} \tag{11}$$

in which

$$k_1 = \frac{A_{X1}\sqrt{2\pi\sigma_{X1}^2}}{A_{X1}\sqrt{2\pi\sigma_{X1}^2} + A_{X2}\sqrt{2\pi\sigma_{X2}^2}} \tag{12}$$

$$k_2 = \frac{A_{X2}\sqrt{2\pi\sigma_{X2}^2}}{A_{X1}\sqrt{2\pi\sigma_{X1}^2} + A_{X2}\sqrt{2\pi\sigma_{X2}^2}}. \tag{13}$$

This means we can regard the normalized Fourier transformation of the X channel as a convex combination of two independent component. Consequently, the Airy term for the X channel can be written as

$$\begin{aligned}F_X = C_0 + 2C_1[&k_1\cos(\phi+\tau a_{X1}d)e^{\frac{-\tau^2\sigma_{X1}^2 d^2}{2}}\\ &+k_2\cos(\phi+\tau a_{X2}d)e^{\frac{-\tau^2\sigma_{X2}^2 d^2}{2}}]\end{aligned} \tag{14}$$

where $\tau = 4\pi\eta_l\cos\theta_2$.

Let $T_{X1}(d) = \cos(\phi+\tau a_{X1}d)e^{\frac{-\tau^2\sigma_{X1}^2 d^2}{2}}$ and $T_{X2}(d) = \cos(\phi+\tau a_{X2}d)e^{\frac{-\tau^2\sigma_{X2}^2 d^2}{2}}$. We have

$$F_X = C_0 + 2C_1[k_1 T_{X1}(d) + k_2 T_{X2}(d)]. \tag{15}$$

Then, the expectation of F_X is given by

$$\mathbb{E}[F_X] = C_0 + 2C_1(k_1\mathbb{E}[T_{X1}] + k_2\mathbb{E}[T_{X2}]). \tag{16}$$

The variance of F_X is given by

$$\begin{aligned}\mathrm{Var}[F_X] &= \mathbb{E}[F_X^2] - \mathbb{E}[F_X]^2\\ &= 4C_1^2(k_1^2\mathbb{E}[T_{X1}^2] + k_2^2\mathbb{E}[T_{X2}^2] + 2k_1k_2\mathbb{E}[T_{X1}T_{X2}])\\ &\quad - 4C_1^2(k_1^2\mathbb{E}[T_{X1}]^2 + k_2^2\mathbb{E}[T_{X2}]^2 + 2k_1k_2\mathbb{E}[T_{X1}]\mathbb{E}[T_{X2}]).\end{aligned} \tag{17}$$

The above equation relies on the expectation of $T_{X1}(d)T_{X2}(d)$, and we derive its analytical expression as follows.

Firstly, we rewrite $T_{X1}(d)T_{X2}(d)$ as

$$\begin{aligned}&T_{X1}(d)T_{X2}(d) = \cos(\phi+\tau a_{X1}d)\cos(\phi+\tau a_{X2}d)e^{\frac{-\tau^2\sigma_X^2 d^2}{2}}\\ &\approx \cos(\phi+\tau a_{X1}d)\cos(\phi+\tau a_{X2}d)(1 - Ed^2 + \frac{Ed^4}{2})\\ &= \frac{1}{2}\cos(2\phi+B_1 d)(1-Ed^2+\frac{Ed^4}{2}) + \frac{1}{2}\cos(B_2 d)(1-Ed^2+\frac{Ed^4}{2})\end{aligned} \tag{18}$$

in which $\sigma_X^2 = \sigma_{X1}^2 + \sigma_{X2}^2$, $B_1 = \tau(a_{X1}+a_{X2})$, $B_2 = \tau(a_{X1}-a_{X2})$, and $E = -\tau^2\sigma_X^2/2$.

Let $T_a(d) = \cos(2\phi + B_1 d)(1 - Ed^2 + \frac{Ed^4}{2})$ and $T_b(d) = \cos(B_2 d)(1 - Ed^2 + \frac{Ed^4}{2})$. Their expectations are given by

$$\begin{aligned}\mathbb{E}[T_a] &= \int T_a(d)P(d)\mathrm{d}d\\ &= \frac{1}{2d_\Delta}(Q_{a1}(d)\cos(2\phi+B_1 d) + Q_{a2}(d)\sin(2\phi+B_1 d))|_{d_{min}}^{d_{max}}\end{aligned} \tag{19}$$

and

$$\begin{aligned}\mathbb{E}[T_b] &= \int T_b(d)P(d)\mathrm{d}d\\ &= \frac{1}{2d_\Delta}(Q_{b1}(d)\cos(B_2 d) + Q_{b2}(d)\sin(B_2 d))|_{d_{min}}^{d_{max}}\end{aligned} \tag{20}$$

respectively. With some algebra, we find that $Q_{a1}(d)$ and $Q_{b1}(d)$ are almost identical to Eq. 16 in the paper except for some differences in notations. For $Q_{a1}(d)$, we only need to replace E_c and B_c with E and B_1, respectively. For $Q_{b1}(d)$, we only need to replace E_c and B_c with E and B_2, respectively. Likewise, $Q_{a2}(d)$ and $Q_{b2}(d)$ are almost identical to Eq. 17 in the paper. A similar replacement

© 2018 The Author(s)
Computer Graphics Forum © 2018 The Eurographics Association and John Wiley & Sons Ltd.

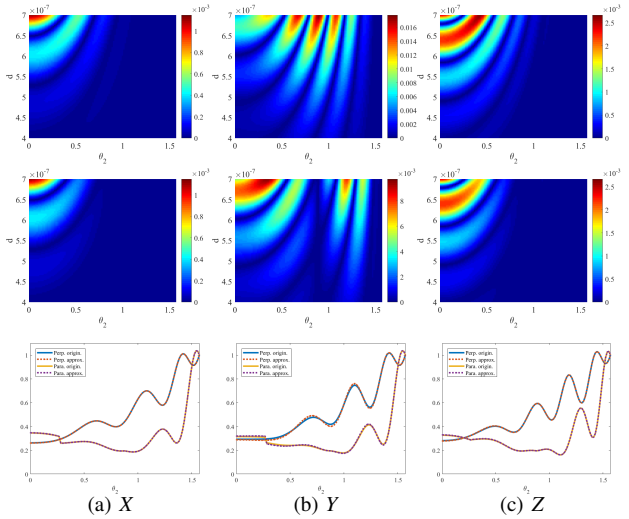

(a) X (b) Y (c) Z

Figure 2: *Additional validation results of the approximated F_c as compared to the original formula. First row: the error maps of F_c for perpendicular polarizations. Second row: the error maps of F_c for parallel polarizations. Third row: 2D profiles comparison of $d = 7e-7nm$. Here, we set $\eta_l = 1.8$.*

is required to obtain the proper formula. After that, the expectation of $T_{X1}(d)T_{X2}(d)$ is given by

$$\mathbb{E}[T_{X1}T_{X2}] = \frac{1}{2}\mathbb{E}[T_a] + \frac{1}{2}\mathbb{E}[T_b]. \tag{21}$$

4. Additional Validation Results of Eq. 13

In this section, we provide additional results to validate the accuracy of the approximated F_c (Eq. 13 in the paper) as compared to the original formula (Eq. 11 in the paper). The refractive index of the thin film is set as $\eta_l = 1.8$. Note that the results are quite similar as compared to the case of $\eta_l = 1.5$ in the paper.

5. Additional Results of the Mean and the Standard Deviation

This section provides additional results to visualize the mean and the standard deviation for the sphere scene. Fig. 3 shows the results in the case of $\eta_l = 1.2$. Two different average thicknesses are considered: $d_{avg} = 500$nm and $d_{avg} = 600$nm. The interval d_Δ ranges from 10nm to 130nm. Fig. 4 shows an anther case in which $\eta_l = 1.8$. Clearly, d_{avg} and η_l determine the hue of the iridescent patterns while d_Δ influences the saturation and the dispersion of the color distribution.

6. Additional Results of the Wave Plane Scene

This section provides additional results of the wave plane scene applied with our appearance model. To test the scope of our model, we use different parameter settings in Fig. 5 and Fig. 6.

References

[BB17] BELCOUR L., BARLA P.: A practical extension to microfacet theory for the modeling of varying iridescence. *ACM Trans. Graph. 36*, 4 (July 2017), 65:1–65:14. 1

© 2018 The Author(s)
Computer Graphics Forum © 2018 The Eurographics Association and John Wiley & Sons Ltd.

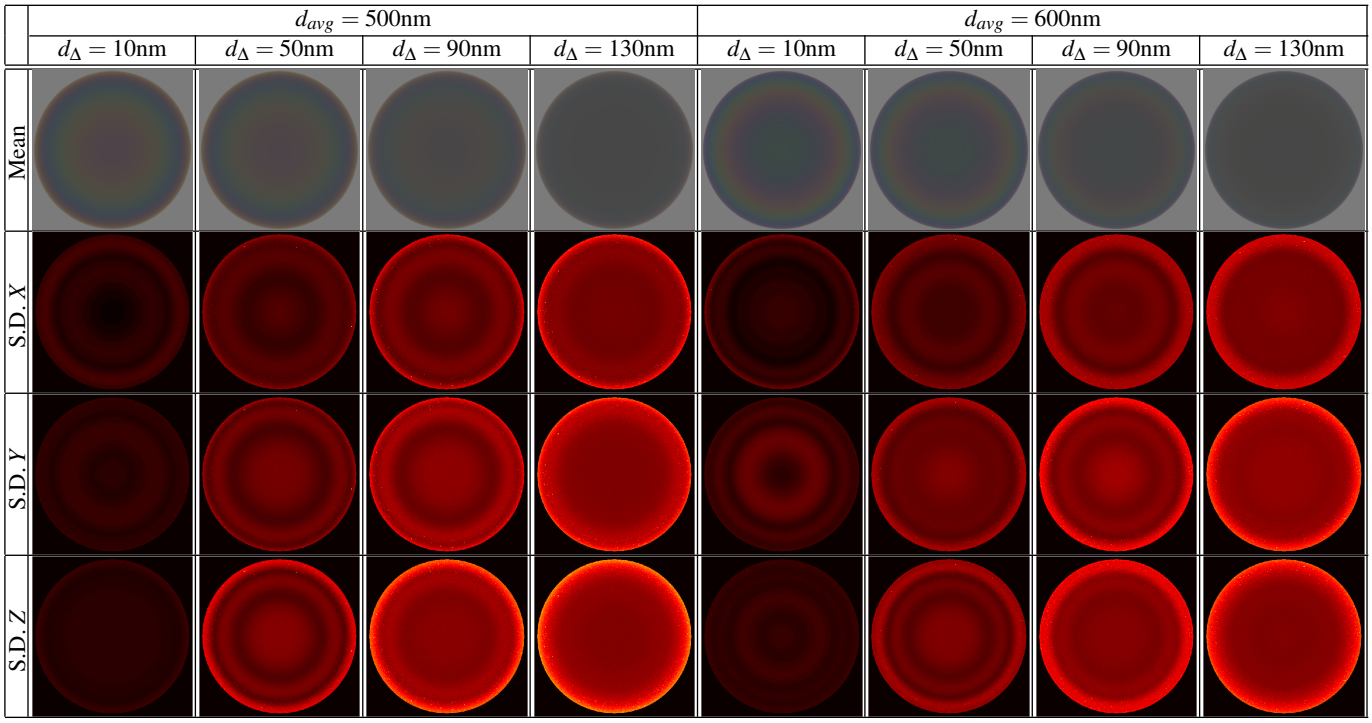

Figure 3: *Visualization of the mean and the standard deviation (in hotmap) for the sphere scene with* $\eta_l = 1.2$.

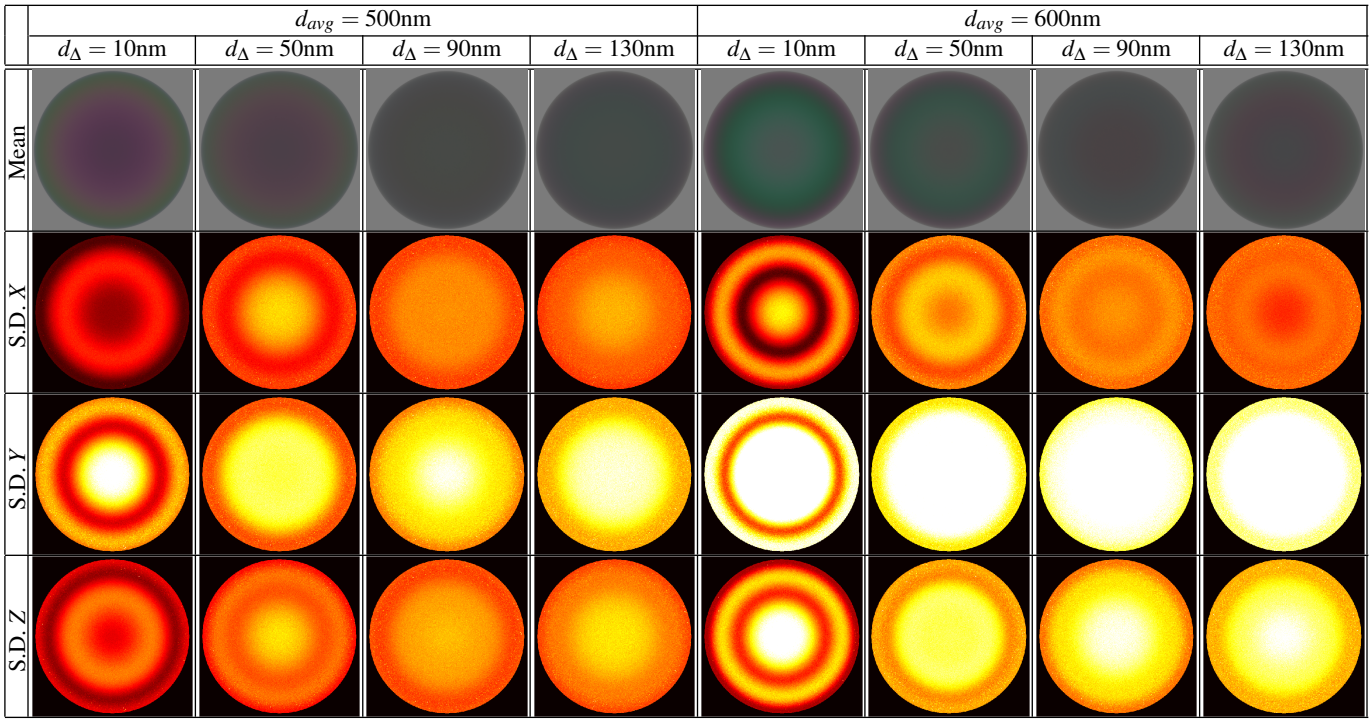

Figure 4: *Visualization of the mean and the standard deviation (in hotmap) for the sphere scene with* $\eta_l = 1.8$.

© 2018 The Author(s)
Computer Graphics Forum © 2018 The Eurographics Association and John Wiley & Sons Ltd.

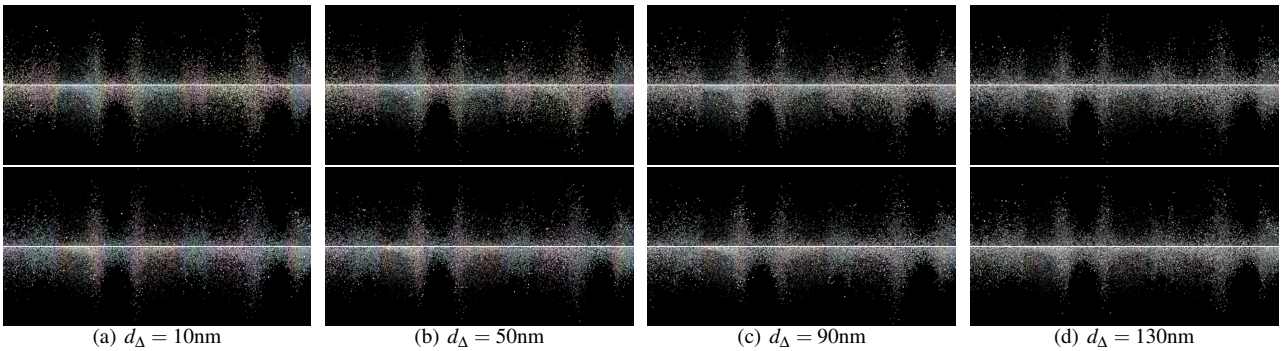

(a) $d_\Delta = 10$nm (b) $d_\Delta = 50$nm (c) $d_\Delta = 90$nm (d) $d_\Delta = 130$nm

Figure 5: *Rendering a wave plane with the proposed BRDF model using increasing values of d_Δ. η_l is set as 1.2 while d_{avg} is set as 500nm (the first row) and 600nm (the second row), respectively.*

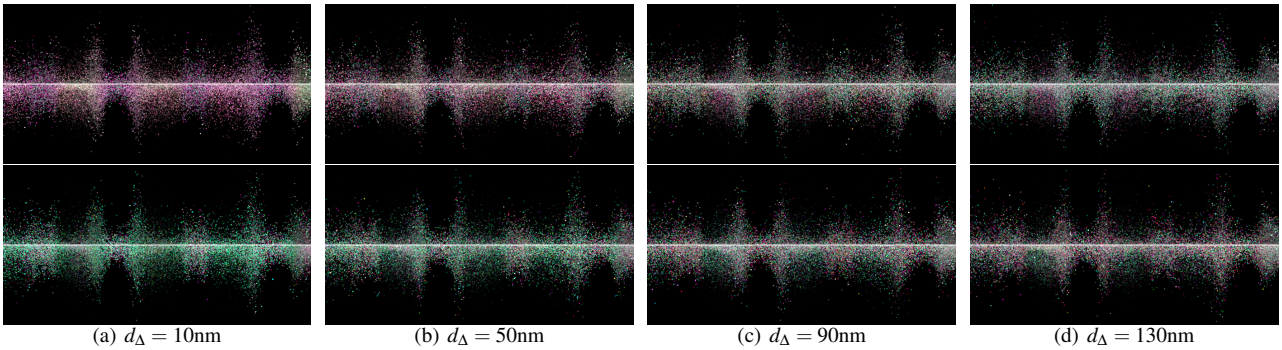

(a) $d_\Delta = 10$nm (b) $d_\Delta = 50$nm (c) $d_\Delta = 90$nm (d) $d_\Delta = 130$nm

Figure 6: *Rendering a wave plane with the proposed BRDF model using increasing values of d_Δ. η_l is set as 1.8 while d_{avg} is set as 500nm (the first row) and 600nm (the second row), respectively.*

© 2018 The Author(s)
Computer Graphics Forum © 2018 The Eurographics Association and John Wiley & Sons Ltd.